High Temperatures-High Pressures, Vol. 49, pp. 125–142
Reprints available directly from the publisher
Photocopying permitted by license only
DOI: 10.32908/hthp.v49.801

Effect of glass transition: density and thermal conductivity measurements of B_2O_3

Dmitry Chebykin[1]*, Hans-Peter Heller[1], Ivan Saenko[2], Gert Bartzsch[1], Rie Endo[3] and Olena Volkova[1]

[1]*Institute of Iron and Steel Technology, TU Bergakademie Freiberg, Leipziger Straße 34, 09599 Freiberg, Germany*
[2]*Institute of Materials Science, TU Bergakademie Freiberg, Gustav-Zeuner-Straße 5, 09599 Freiberg, Germany*
[3]*Department of Materials Science and Engineering, Tokyo Institute of Technology, 152–8552 Tokyo, Japan*

Received: May 28, 2019; Accepted: October 11, 2019.

The role of B_2O_3 as a fluxing agent for developing fluoride free fluxes has been accentuated in the recent years. Therefore, knowledge about thermophysical properties of the oxide are essential to find the optimal chemical composition of the mold fluxes. In the present study, the density and thermal conductivity of B_2O_3 were measured by means of the buoyancy method, the maximal bubble pressure (MBP) method and the hot-wire method in the temperature range of 295–1573 K. The results are discussed in the context of the chemical stability of the B_2O_3 as well as the effect of glass transition on the thermal conductivity. The density of the B_2O_3 decreases non-linearly with increasing temperature in the temperature range of 973–1573 K. The MBP method was successfully applied for the density measurements with a viscosity up to 91 Pa.s. The thermal conductivity of the B_2O_3 in the solid and molten states increases with increasing temperature. Based on the Kittel's equation, the temperature dependence of the thermal conductivity through the glass transition temperature of B_2O_3 was discussed.

Keywords: Boron trioxide, B_2O_3, density, thermal conductivity, buoyancy method, hot-wire method, maximum bubble pressure method, glass transition

*Corresponding author: Dmitry.Chebykin@iest.tu-freiberg.de

1 INTRODUCTION

Appropriate viscosity and thermal conductivity of mold fluxes are necessary to ensure optimal continuous steel casting conditions. These properties support the increase of productivity of steel plants without surface defects, such as sticker breakouts as well as longitudinal cracking [1–3]. In order to minimize these defect formations, commercial mold fluxes are based on the $CaO\text{-}SiO_2\text{-}Al_2O_3$ ternary system with addition of fluorite and sodium carbonate. The additivities are responsible for the reduction of both melting temperature and viscosity as well as for the reduction of the heat transfer by forming cuspidine ($3CaO.2SiO_2.CaF_2$) [4]. Thereby, the rapid crystallization of a flux film brings a stable mild cooling effect of the mold [4].

On the other hand, these fluorides cause environmental hazards, the safety issue and the plant corrosion [2]. It is necessary to find slag compositions, which have the same properties (e.g. viscosity, melting temperature and thermal conductivity) as fluxes containing fluorides. The importance of B_2O_3 together with these components as a fluxing agent for the development of fluoride free fluxes has been acknowledged in the recent years. The influence of B_2O_3 on the viscosity of slags has been widely investigated [2,5–11]. Generally, addition of B_2O_3 leads to a decrease in the slag viscosity. On the other hand, B_2O_3 can inhibit the mold flux crystallization [2,9,11,12]. Due to increasing the incubation time, the structure of mold fluxes tends to be predominantly glassy [11], suggesting that the mold flux exists as molten and glassy solid states between the steel shell and the mold. Therefore, knowledge about thermal conductivity is required for both molten and glassy solid state of the mold flux containing B_2O_3. However, the effect of B_2O_3 on the thermal conductivity of fluxes has been studied only in few investigations [13–17] and all of which have been conducted only for the molten systems. Furthermore, the temperature dependence of the thermal conductivity has not been reported even for solid B_2O_3. Shurygin et al. [18] and Kim et al. [19] reported the thermal conductivity of molten B_2O_3 in temperature ranges of 1200–1400 K and 873–1373 K, respectively. However, there is a large discrepancy. Nilsson et al. [20] measured the thermal conductivity of B_2O_3 at 300–1000 K under high pressure of 0.1 and 0.2 GPa. Thus, there has been no report for thermal conductivity of B_2O_3 under normal pressure in the temperature range from 298 to 873 K, including the glass transition temperature of B_2O_3 (around 580 K [21]). It is known that temperature coefficients of the volume and enthalpy change around the glass transition temperature, the temperature coefficient of the thermal conductivity would also change [22,23]. It is essential for the basic understanding of thermal conductivity of B_2O_3 for further investigation of systematic measurement of the thermal conductivity of B_2O_3 containing system.

Thus, the present work aims to measure the thermal conductivity of B_2O_3 both in glassy and molten state and to investigate the effect of glass transition on the thermal conductivity.

2 EXPERIMENTAL

In this study, the thermal conductivity was measured by the transient hot-wire method. The thermal diffusivity also provides thermal conductivity as a product of density and heat capacity. Ogura et al. [24] reported the thermal diffusivity of molten B_2O_3 measured by the laser flash method. Thus, to compare the measured data with reported values, the density of B_2O_3 was also measured.

2.1 Thermal conductivity measurement

Figure 1 a) shows the schematic diagram of a measuring cell, which was applied for the thermal conductivity measurements. A Pt-13%Rh wire with a diameter of 0.15 mm was used for a heater. A constant heat flux is generated from the heater by applying a constant current. The temperature rise (ΔT) of the hot-wire was recorded continuously by two potential leads. On the basis of the solution for the continuous source of heat by Carslaw and Jaeger [25], the thermal conductivity of the sample was calculated from Eq. (1):

$$\lambda = \frac{\dot{Q}}{4\pi} / \frac{d\Delta T}{d\ln(t)} \tag{1}$$

where $\dot{Q}$ is the heat generation rate per unit length of the hot-wire and t is the measurement time.

It is essential for calculating the thermal conductivity to determine two parameters: (i) slope between the temperature change and the natural logarithm of time ($d\Delta T/d\ln(t)$) and (ii) heat flux density ($\dot{Q}$). In the technique, the heater in Figure 1 a) is used not only as a heating element but also for temperature measurements. The temperature change (ΔT) is determined as the resistance change of the heater, which was recorded as the voltage change (ΔU) on the basis of four-terminal method. As a result, the thermal conductivity can be calculated using Eq. (2):

$$\lambda = \frac{I^3 \cdot r_T \cdot X \cdot R_{298}}{4\pi} \Big/ \frac{d\Delta U}{d\ln t} \tag{2}$$

$$X = \frac{R_{298}}{l_{hot-wire}} \tag{3}$$

where I is the supplied current, R_{298} is the resistance of the hot-wire between potential leads at room temperature, $l_{hot\text{-}wire}$ is the length of the hot-wire, r_T and R_T are the temperature coefficient of electrical resistivity and the resistances of the hot-wire between potential leads at the temperature of interest T, respectively.

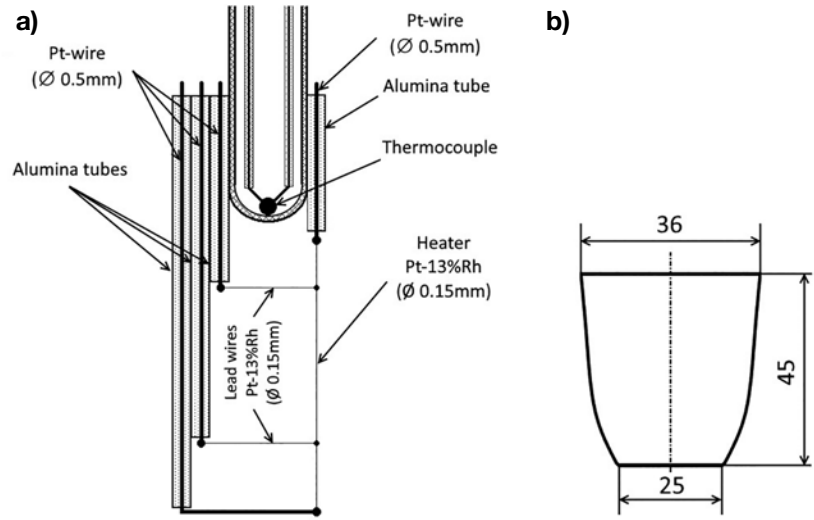

FIGURE 1
Schematic drawings of **a)** the hot-wire for determination of thermal conductivity and **b)** geometrical parameters of platinum crucible in mm used for hot-wire method.

The B_2O_3 sample in a platinum crucible (Figure 1 b) was heated in a resistance furnace up to 973 K with the heating rate of 3–5 K/min and held around 1 h. The furnace temperature was controlled by a protected thermocouple (type K), which was directly immersed into the sample. Afterwards, the measuring cell was gently immersed into the molten B_2O_3 due to the high viscosity of the melt (91 Pa.s [26]). Subsequently, the system was additionally held for 30 min and cooled down to 298 K during 12 h. The thermal conductivity measurements were conducted from 298 to 973 K. The holding time at each temperature was 30 min after reaching the measurement temperature. Then, the thermal conductivity measurements were started by applying a current of 1.0 A. The voltage change of the heater was recorded by a digital multimeter, which was controlled by a PC software, as a function of time. Measurements were conducted 3 to 5 times in order to ensure the reproducibility of the results. The accuracy of this technique was confirmed by the measurement of water. The deviation from the recommended values in [27,28] was lower than 2%.

2.2 Density measurements

2.2.1 Buoyancy method

Density measurements of the molten B_2O_3 were conducted by means of the buoyancy method (Archimedes' Principle) and the maximum bubble pressure method (MBP) in the temperature range of 973–1573 K. Figure 2 shows the schematic diagram of the induction furnace for density measurements by means of the buoyancy method. According to Archimedes' principle (direct method), the density of the molten B_2O_3 ($\rho_{B_2O_3}$) can be calculated using Eq. (4):

$$\rho_{B_2O_3} = \frac{\Delta W}{V_{Bob}} = \frac{W_{bob}^{air} - W_{bob}^{liquid}}{V_{Bob}} \tag{4}$$

where ΔW is the change of the weight before (W_{bob}^{air}) and after immersion (W_{bob}^{liquid}) of the bob into the molten B_2O_3, V_{Bob} is the volume of the bob.

Figure 3 a) shows the geometrical parameters of bobs used in the present work.

Two molybdenum bobs with volumes of 0.582 and 0.223 cm^3 (V_{Bob_1} and V_{Bob2}, respectively) were immersed into the molten B_2O_3 in order to reduce the effect of the surface tension on the buoyancy forces. The weight change before and after the immersion was measured by the analytical balance with the readability of 0.01 mg. Before the immersion, the weight of bodies above the melt was set to a new zero. After this procedure, the bodies were immersed into the melt. The average weight change used for calculating the density at the temperature T ($\rho_{B_2O_3}^T$) was become from the values recorded during 5 min. As a result, the density of the B_2O_3 was calculated using following equation:

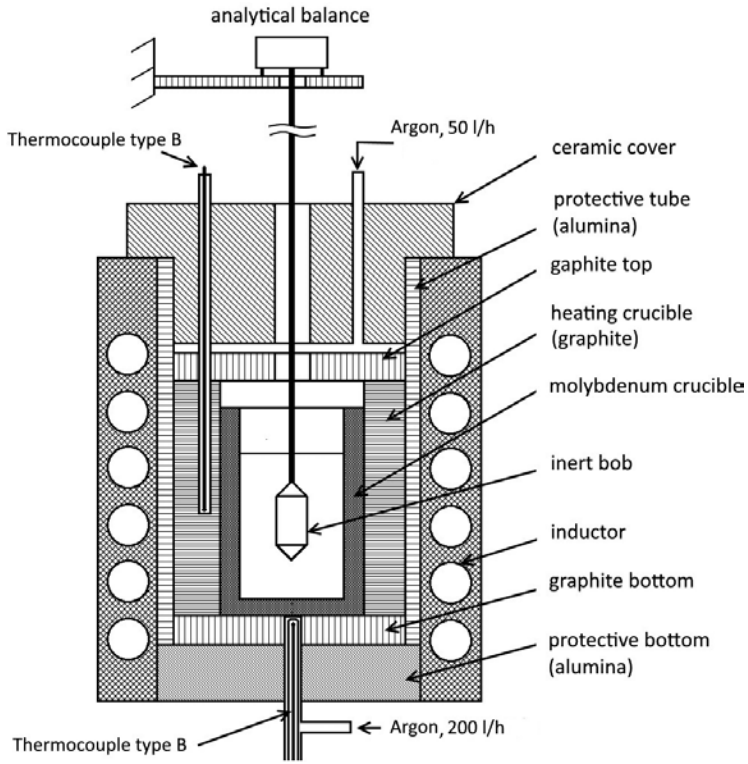

FIGURE 2
Schematic diagram of the induction furnace for the determination of density.

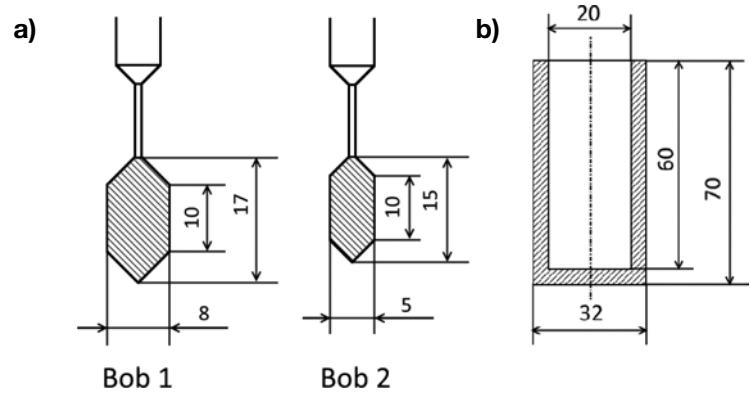

FIGURE 3
Geometrical parameters of **a)** molybdenum bobs for the density measurements by the buoyancy method and **b)** molybdenum crucible (> 99.97% Mo) in mm.

$$\rho^{T}_{B_2O_3} = \frac{\Delta W_{Bob_1} - \Delta W_{Bob_2}}{V_{Bob_1} - V_{Bob_2}} = \frac{\Delta W_{Bob_1} - \Delta W_{Bob_2}}{\Delta V_T} \tag{5}$$

where ΔV_T is the volume difference between the molybdenum bobs at the temperature T, subscripts Bob_1 and Bob_2 represent large and small bobs, respectively.

The volume difference at each temperature can be expressed using Eq. (6):

$$\Delta V_T = \Delta V_{293} \cdot (1 + 3 \cdot \alpha \cdot (T - T_{293})) \tag{6}$$

where α is the linear thermal expansion coefficient. The volume difference of the bodies at the room temperature (ΔV_{293}) was measured using distilled water. According to the technical data, the coefficient of the linear thermal expansion for the molybdenum amounts $5.2 \cdot 10^{-6}$ K^{-1} at 293 K [29]. This value was considered as a constant in the measurement temperature range [30].

Before the measurement, 25 g of B_2O_3 sample was melt in a molybdenum crucible as shown in Figure 3 b) at 1023 K in Ar (99.999 vol.% Ar, < 2 ppm O_2) and cooled. The heating rate was 5 K/min, holding time was 1 h. In the measurement, the sample in the molybdenum crucible was heated to 1573 K with a heating rate of 30 K/min and Ar flow rate of 250 l/h (200 l/h from bottom and 50 l/h from top of the crucible). As shown in Figure 2, the temperature field in the molybdenum crucible was controlled using a thermocouple type B (bottom). In order to ensure a correct temperature control, a thermocouple type K was directly immersed into the melt before the experiment. After holding for 1 h, the measurement was started. During the experiment with the melt, a flow rate of Ar was set to the level of 0 l/h in

order to exclude an additional buoyancy force and obstructions to the movement of the rod. Each measurement took at least 5 min and was repeated 3 times with a time interval of 10 min. The measurements were carried out in temperature range of 1073 to 1573 K in the cooling cycle after holding longer than 30 min at each temperature.

2.2.2 MBP method

In addition to the investigation of the density by means of the buoyancy method, the density was measured by the maximum bubble pressure method (MBP). The technique was described elsewhere [31] in detail. In the method, the density was calculated by applying Eq. (7):

$$P_{max} = P_{\gamma} + \rho \cdot g \cdot h = \frac{4 \cdot \gamma}{d} + \rho \cdot g \cdot h \tag{7}$$

where P_{max}, P_{γ}, g, h, γ and d represent the maximum bubble pressure, pressure in the bubble, density, gravitational acceleration, immersion depth, surface tension and diameter of the capillary tube, respectively.

For these measurements, a molybdenum capillary with the inner diameter of 2.5 mm was used. The capillary tube in the molten sample was flushed by Ar with a flow rate of 0.2 ml/min (1–2 bubbles per a minute). Using a pressure transmitter, the total pressure was measured. Herewith, the maximal bubble pressure was determined. The measurements were carried out at the immersion depth (h) of 10 to 20 mm with the step of 2 mm. The capillary was immersed up to 21 mm and then lifted up to 10 mm with a step of 2 mm. The position of the capillary in the melt was controlled by a hydraulic sensor. The resolution of the sensor was 0.001 mm. The crucible and experimental conditions were almost same as those for the buoyancy method. The measurements were carried out in the cooling cycle in the temperature range of 973 to 1573 K.

2.3 Analysis of B_2O_3 sample

The chemical composition of the B_2O_3 sample after the thermal conductivity experiments was analyzed by X-ray fluorescence (XRF) spectroscopy.

Differential scanning calorimetry measurement (DSC) was performed from RT up to 673 K to confirm the glass transition temperature. The B_2O_3 sample was heated up in dried Ar atmosphere in Pt/Rh crucible with heating rate of 10 K/min.

X-ray powder diffraction (XRD) has been performed using a diffractometer with the graphite monochromator and the CuKα radiation (α = 1.5418 Å). The goniometer of the diffractometer had the Bragg-Brentano geometry. During measurement, powder samples were placed on the monocrystalline silicon substrate with (510) orientation. In this case, the orientation of the substrate does not show any peak on the XRD pattern in the range of 15–110° of 2θ.

3 RESULTS

3.1 Thermal conductivity

The typical voltage change (see in Figure 4) represents the thermal conductivity measurement at 973 K with a current supply of 1.0 A. The origin of the time is the timing of the issue a command to supply the current and to start the data acquisition. However, it takes 60 ms for a power operational amplifier to achieve the current to the objective value of 1.0 A. Thus, Eq. (2) was modified into following equation:

$$\lambda = \frac{I^3 \cdot \alpha_T \cdot X \cdot R_T}{4\pi} \Big/ \frac{d\Delta U}{d\ln(t_{corr})} \tag{8}$$

$$t_{corr} = t - 0.06 \tag{9}$$

where t_{corr} is the corrected time.

Figure 5 shows the schematic voltage change (ΔU) as a function of the logarithmic time $\ln(t)$. The curve in Figure 5 can be divided into three different regions: a first unstable region caused by the initial current supply or by the heat capacity of the hot-wire; a second stable region; a third region – where natural convection already occurs [32–34]. Only the linear slope in the second stable region can be used for calculating the thermal conductivity. In Figure 4, the linear slope can been seen between ΔU and $\ln(t)$ in the range of

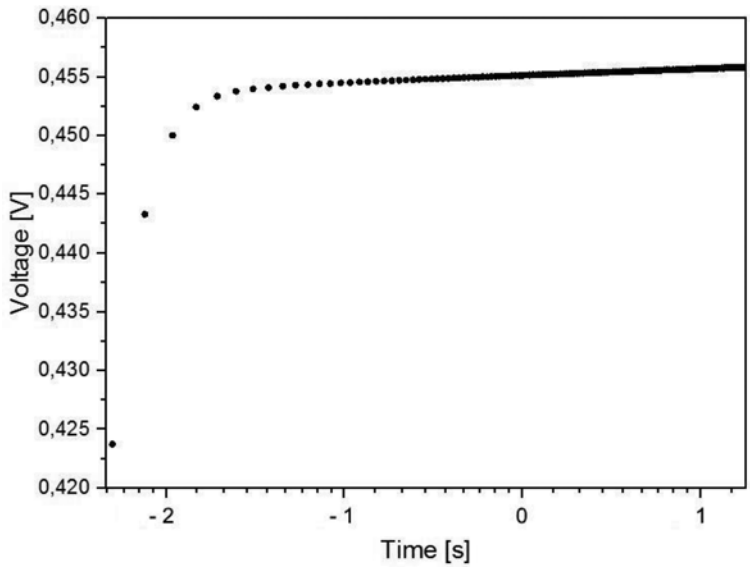

FIGURE 4
Typical voltage change during the experiment at the temperature of 973 K.

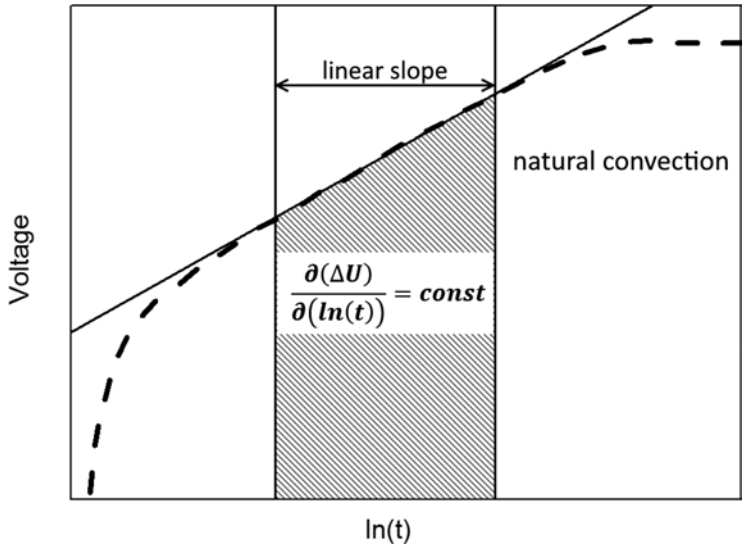

FIGURE 5
Schematic diagram of the voltage change as a function of logarithmic time.

$-1.0 < \ln(t) < 1.0$. This region can be used for the determination of the thermal conductivity.

Figure 6 shows the temperature dependence of the thermal conductivity for B_2O_3 measured in this study. The comparison with other reported data and the temperature dependence will be discussed later.

3.2 Density

The density of the molten B_2O_3 measured by the buoyancy method and the MBP method is presented in Figure 7 and in Table 1. It was found that the density of the B_2O_3 decreases non-linearly with increasing temperature. The results from two different methods show good agreement. Also, no significant difference was found between the present results and Napolitano et al. [26] as well as Riebling [35].

3.3 Sample analysis

Botta et al. [21] reported that the glass transition temperature was around 580 K for B_2O_3. To confirm the glass transition temperature for the B_2O_3 sample used in this study, DSC and XRD analysis were conducted. Figure 8 and Figure 9 show the obtained DSC and XRD profiles, respectively. The DSC result shows an endothermic reaction at 537 K, which is the glass transition temperature for the sample [21]. The data are good related with the temperature reported by Botta et al. [21]. Figure 9 shows that both samples are considered to be glassy and no obvious change was found by the heat treatment up to 523 K.

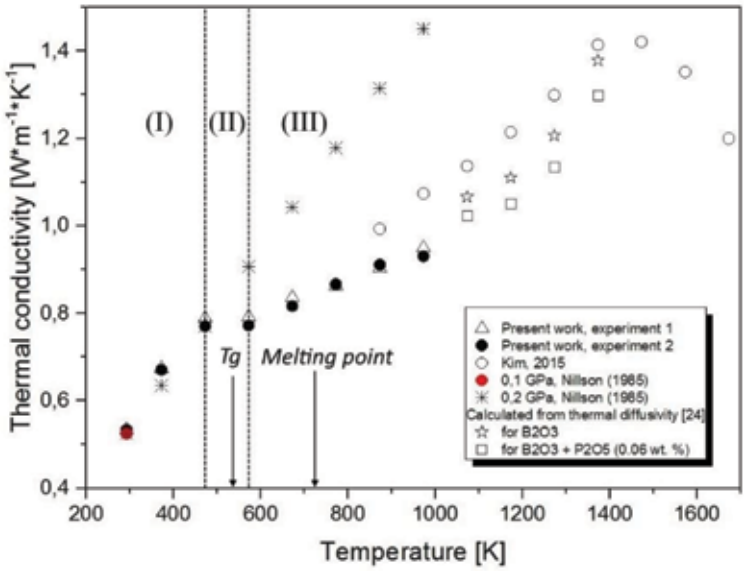

FIGURE 6
Thermal conductivity of B_2O_3 compared with values reported by Kim et al. [19], Nilsson et al. [20] and calculated from thermal diffusivity of B_2O_3 and B_2O_3-P_2O_5 (0.06 wt. %) [24].

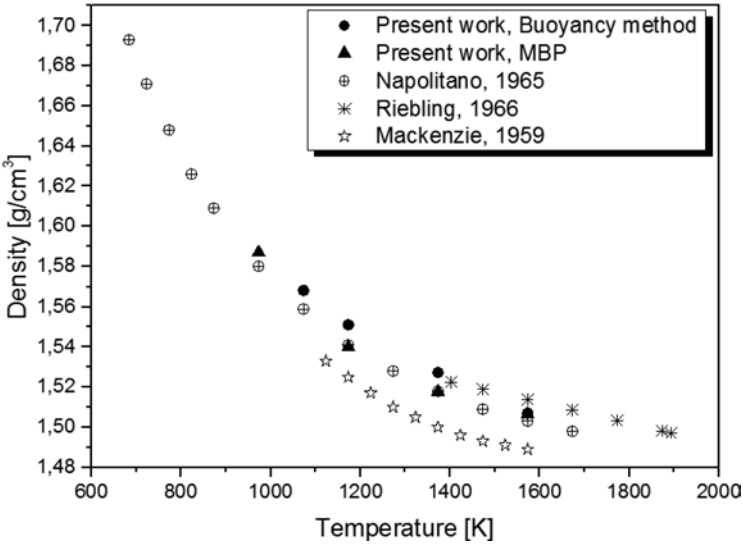

FIGURE 7
Temperature dependence of density for the molten B_2O_3 measured by buoyancy method and MBP method compared with values reported by Napolitano et al. [26], Riebling [35] and Mackenzie [36].

TABLE 1
Density of the B_2O_3.

Temperature/K	buoyancy method/gcm^{-3}	MBP method/gcm^{-3}
1573	1.507	1.506
1373	1.527	1.518
1173	1.551	1.540
1073	1.568	–
973	–	1.587

Table 2 shows the chemical composition of the B_2O_3 sample after the measurement. The sample contains other oxides with the total amount of 0.5 mass%.

4 DISCUSSION

4.1 Density measurements

In this study, the density of the B_2O_3 was measured by the buoyancy and the MBP methods. The measured data by these techniques are in good agreement in the temperature range of 1173–1573 K. At 973 K, the density measurement by means of the MBP method was complicated due to the high viscosity of

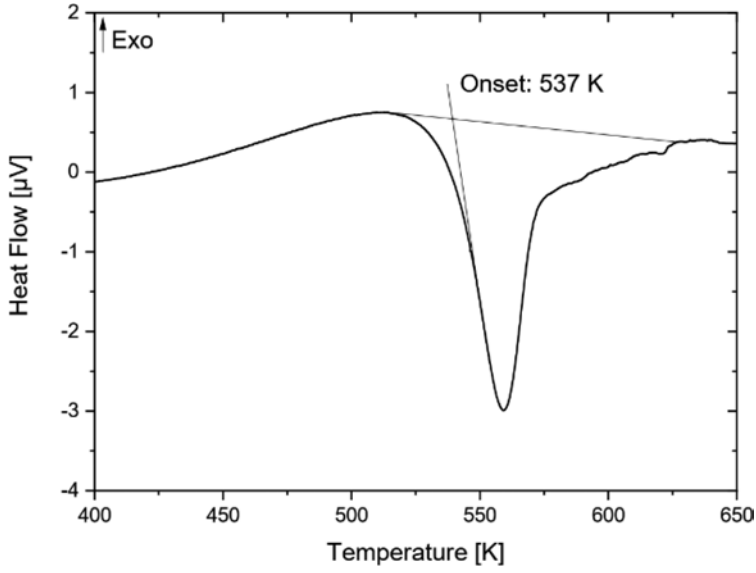

FIGURE 8
DSC measurement of B_2O_3 sample.

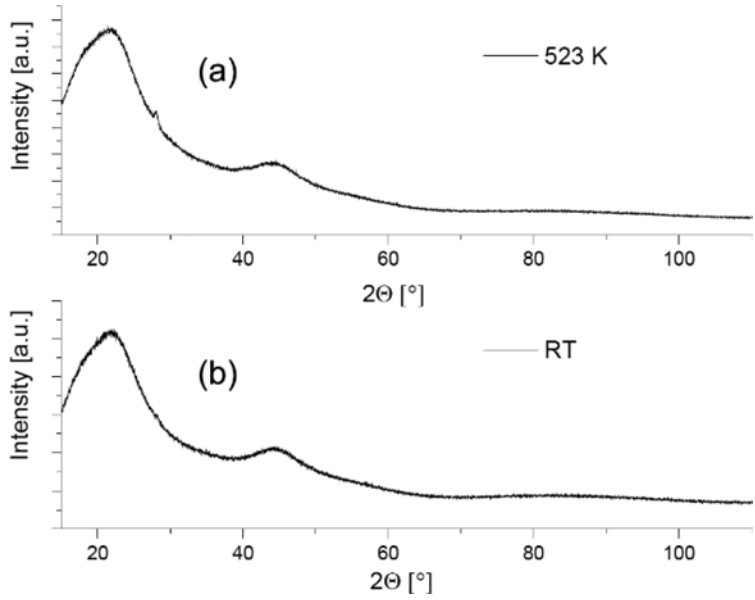

FIGURE 9
XRD-profiles for samples: (a) after heated up to 523 K and (b) as-obtained.

TABLE 2
Chemical composition of the B_2O_3 after the thermal conductivity measurements in mass%.

B_2O_3	SiO_2	P_2O_5	CaO	MnO	Fe_2O_3	WO_3
99.5	0.14	0.09	0.02	0.05	0.01	0.13

the molten B_2O_3 [26]. The measured signal was very unstable at different flow rates of Ar in the range of 0.150 to 0.500 ml/min.

In spite of that, this method show an excellent agreement with the values reported by Napolitano et al. [26] and Riebling [35]. The density measurement by the buoyancy method could not be conducted at 973 K due to the high viscosity of the sample. The results achieved by the buoyancy method slightly exceed the published values. However, they are in consistency with other works [26,35,36]. The discrepancy between the measured by the buoyancy method and the recommended values can be explained by the insufficient holding time (10 min). The experiments were conducted using two bodies during two days. In spite of the fact, these results show higher discrepancy than the MBP method. Furthermore, the values of the density, which were measured by means of only one body with the volume of 0.582 cm^3, are better related with the recommended values than with two bodies. On the basis of above results, the MBP data were taken for calculating the thermal conductivity of the B_2O_3 from the thermal diffusivity [24].

4.2 Thermal conductivity

4.2.1 Thermal conductivity measurements

This paper firstly focuses on measuring the thermal conductivity of B_2O_3 under normal pressure in the temperature range of 298 K to 973 K. Based on different slopes, the measured values can be divided into three regions: (I) 298–473 K, (II) 473–573 K and (III) over 573 K. In the first and the third regions, the thermal conductivity shows positive temperature dependence; while in the second region, the thermal conductivity tends to become constant values.

In the first temperature range, the thermal conductivity can be calculated by Eq. (10) after a linear fit:

$$\lambda = 0.131 + 1.39 \cdot 10^{-3} \cdot T \tag{10}$$

In the third temperature range, the thermal conductivity is expressed by following equation:

$$\lambda = 0.558 + 0.396 \cdot 10^{-3} \cdot T \tag{11}$$

The difference between the measured and published values in Figure 6 can be caused by the use of different experimental apparatus and different experimental parameters. Nilsson et al. [20] measured the thermal conductivity of B_2O_3 under pressure up to 1.7 GPa using a hot-wire technique. These experiments were carried out in alumina crucibles with nickel hot-wires with a diameter of 0.1 mm. In the temperature range of 298 K to 473 K, results presented by Nilsson et al. [20] and the measured values in the present study are good related. This suggests that even such a high pressure of 0.2 GPa up to 473 K does not play any significant role on the thermal conductivity of solid B_2O_3. Kim et al. [19] used the hot-wire method for determining the thermal conductivity of molten B_2O_3. Experiments were carried out in alumina crucibles using the hot-wire (Pt-13%Rh) with a diameter of 0.15 mm. Hence, the experimental apparatus of the hot-wire method in the present study is similar to that in Kim's work [19]. The difference between the results at the temperature of 873 K amounts 8.7%. The difference in the results with other works [18,20] might be caused by different factors such as different holding time for ensuring the thermal equilibrium of the system at each temperature, the temperature control, the measurement step, the resolution of the equipment and the change in the chemical composition due to the dissolution of the alumina crucible.

As mentioned in 3.3, the sample had 0.13 mass% of WO_3 and 0.14 mass% of SiO_2 after the thermal conductivity measurement. The existence of the oxides in the sample was caused by the sample preparation for the chemical analysis. On the other hand, the sample has a relative high content of P_2O_5 (0.09 mass%), which cannot be explained by the sample preparation.

Therefore, the thermal conductivity was calculated according to Eq. (12) from the thermal diffusivity reported by Ogura et al. [24] for B_2O_3 and for B_2O_3-P_2O_3 (0.06 mass%) samples to evaluate the effect of the contamination, which values are also included in Figure 6.

$$\lambda = a \cdot \rho \cdot C_p \tag{12}$$

where a, ρ and C_p represent the thermal diffusivity, density, heat capacity, respectively.

In this calculation, the used density was measured in this study and the heat capacity for B_2O_3 was taken from a literature [37]. The calculated thermal conductivity is in good agreement with the calculated values for the B_2O_3 with 0.06 mass % of P_2O_5. Thus, the contamination of other oxides is considered not to effect to the thermal conductivity measurement.

4.2.2 Influence of glass transition on thermal conductivity

Kim et al. [19] reported that the thermal conductivity of molten B_2O_3 can be understood by following equation [38]:

$$\lambda = \frac{1}{3} \cdot C_V \cdot v \cdot l \tag{13}$$

where *Cv* is the heat capacity at constant volume, *v* is the speed of sound and *l* is the mean free path of phonon. Kim et al. [19] calculated the phonon mean free path of the B_2O_3 from references [22,26,39] using Eq. (13). In the temperature range of 873–1273 K, the mean free path of phonon increases from 0.87 to 1.20 nm with increasing temperature. It was concluded that the parameter is responsible for increasing the thermal conductivity in this temperature range. It is expected that the mean free path of phonon can be related with the structure change [19].

In the third temperature range of 573 K to 973 K, the sample was also liquid. Hence, in this section, the discussion starts from the third temperature region for molten B_2O_3 to check whether the phonon mean free path is still dominant factor of the temperature dependence for the thermal conductivity at temperature lower than 873 K.

Figure 10 shows the temperature dependence of the thermal conductivity, the heat capacity, the sound of velocity and the mean free path of phonon. The heat capacity (C_v) was calculated as a product of the density and the specific heat of B_2O_3 from references [26,37,40,41]. The density at the glass transition temperature was determined by the extrapolation of data reported by Macedo et al. [40] and Napolitano et al. [26]. The average sound velocity was derived from longitudinal and transverse waves [39,41]. As a result, the mean free path of phonon was calculated using Eq. (13).

In the third region, the mean free path of phonon rises. Whereas, the speed of sound in the molten B_2O_3 and the heat capacity decreases (Figure 10). As

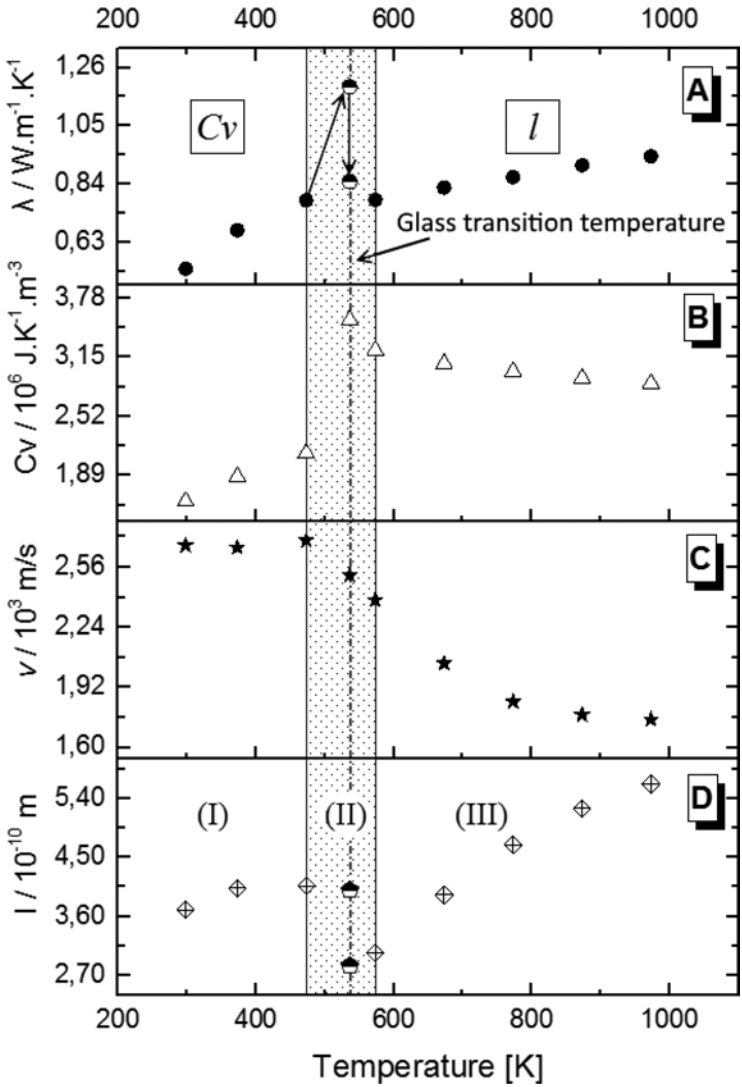

FIGURE 10
Influence of the heat capacity (B) calculated from [26,37,40,41], the speed of sound (C) [39,41] and the mean free path of phonon (D) on the thermal conductivity of the B_2O_3 (A) at different temperatures.

a result, only the phonon mean free path can be responsible for increasing the thermal conductivity in the temperature range of 573–973 K.

In the first region (below 473 K), Figure 10 shows that the significant increase of the heat capacity determines the thermal conductivity slopes. In the second region (between 473 and 573 K), the glass transition influences

the results. As presented in Figure 10, the heat capacity increases sharply up to the glass transition temperature and then starts to decrease. The sound of velocity continuously decreases. The mean free path of phonon around T_g was assumed as follows: the first value just below T_g was taken as 0.40 nm. After overcoming the temperature, the mean free path of phonon was extrapolated to the glass transition temperature from the linear slope of the mean free path of phonon in the temperature range of 573–973 K. It was found that the mean free path of phonon sharply decreases after overcoming the glass transition temperature. The data (C_v, v and l) were applied for calculating the thermal conductivity of B_2O_3 in the second region. As a result, the thermal conductivity of the B_2O_3 just below the glass transition temperature could increase sharply to the maximal value and after that decreases to the value almost same as that before the glass transition.

Based on the above facts, it can be concluded that below the glass transition temperature of the B_2O_3, the thermal conductivity is mainly determined by a change in the heat capacity. Over this temperature, the temperature dependence of the thermal conductivity is affected by the mean free path of phonon. Just above the glass transition temperature, all of these parameters (C_v, v and l) are responsible for decreasing the thermal conductivity.

5 CONCLUSIONS

In the present study, the density and thermal conductivity of B_2O_3 were measured by means of the buoyancy method, the maximal bubble pressure method and the hot-wire method in the temperature range of 295–1573 K. The results are discussed in the context of high temperature calibration errors and the chemical stability of the B_2O_3 as well as the difference in measurement methods. The main results can be summarized as follows:

- Density of the B_2O_3 was successfully measured by the MBP and the buoyancy method. The experimental data are good related with each other and the published values in literature
- Density of the B_2O_3 decreases non-linearly with increasing temperature in the temperature range of 973–1573 K
- The MBP method was successfully applied for the density measurements with a viscosity up to 91 Pa.s
- Thermal conductivity of the B_2O_3 was measured under normal pressure by the transient hot-wire method in the temperature range of 298 K to 973 K
- Thermal conductivity of the B_2O_3 in the solid and molten states increases with increasing temperature
- Based on the Kittel's equation, the theoretical temperature dependence of the thermal conductivity of B_2O_3 through the glass transition temperature was discussed. Below the glass transition temperature of B_2O_3, a change in

the heat capacity mainly influences the thermal conductivity. On the other hand, just above the glass transition temperature, all of these parameters (C_v, v and l) account for decreasing the thermal conductivity. Over this temperature, the temperature dependence of the thermal conductivity is explained by that of the mean free path of phonon.

ACKNOWLEDGMENTS

The contributions of M.A. Kaufmann for academic paper writing to the present work are gratefully acknowledged. Thanks are extended to the European Social Fund (ESF) for financial support of this research.

REFERENCES

[1] Brimacombe, J. K., and Sorimachi, K. *Metall. Trans. B*, **8** (1977), 489, https://doi.org/10.1007/BF02696937.
[2] Fox, A. B., Mills, K. C., Lever, D., Bezerra, C., Valadares, C., Unamuno, I., Laraudogoitia, J. J., and Gisby, J. *ISIJ Int.*, **45** (2005), 1051, https://doi.org/10.2355/isijinternational.45.1051.
[3] Blazek, K. E., and Saucedo, I. G. *ISIJ Int.*, **30** (1990), 435, https://doi.org/10.2355/isijinternational.30.435.
[4] Hanao, M., Kawamoto, M., and Watanabe, T. *ISIJ Int.*, **44** (2004), 827, https://doi.org/10.2355/isijinternational.44.827.
[5] Wen, G., Sridhar, S., Tang, P., Qi, X., and Liu, Y. *ISIJ Int.*, **47** (2007), 1117, http://dx.doi.org/10.2355/isijinternational.47.1117.
[6] Wang, Z., Shu, Q., and Chou, K. Steel Res. Int., **84** (2013), 766, https://doi.org/10.1002/srin.201200256.
[7] Cui, Y., Wang, L., Yang, J., Zhang, J., Sasaki, Y., and Ostrovski, O. *Steel Res. Int.*, **86** (2015), 662, https://doi.org/10.1002/srin.201400354.
[8] Yu, X., Wen, G. H., Tang, P., and Wang, H. *Ironmak. Steelmak.*, **36** (2009), 623, https://doi.org/10.1179/174328109X461419.
[9] Li, G., Wang, H., Dai, Q., Zhao, Y., and Li, J. *J. Iron Steel Res. Int.*, **14** (2007), 25, https://doi.org/10.1016/S1006-706X(07)60006-5.
[10] Qi, X., Wen, G.-H., and Tang, P. *J. Iron Steel Res. Int.*, **17** (2010), 6, https://doi.org/10.1016/S1006-706X(10)60105-7.
[11] Shu, Q., Wang, Z., Klug, J. L., Chou, K., and Scheller, P. R. *Steel Res. Int.*, **84** (2013), 1138, http://dx.doi.org/10.1002/srin.201200341.
[12] Zhou, L., Wang, W., Wei, J., and Lu, B. *ISIJ Int.*, **53** (2013), 665, https://doi.org/10.2355/isijinternational.53.665.
[13] Kim, Y., and Morita, K. *ISIJ Int.*, **54** (2014), 2077, https://doi.org/10.2355/isijinternational.54.2077.
[14] Kim, Y., Yanaba, Y., and Morita, K. *J. Non-Cryst. Solids*, **415** (2015), 1, https://doi.org/10.1016/j.jnoncrysol.2015.02.008.
[15] Kim, Y., and Morita, K. *J. Am. Ceram. Soc.*, **98** (2015), 3996, https://doi.org/10.1111/jace.13820.
[16] Nishi, T., Tanaka, K., Ohnuma, K., Manako, T., Ohta, H., Sukenaga, S., Shibata, H., and Kakihara, T. *J. Nucl. Mater.*, **510** (2018), 193, https://doi.org/10.1016/j.jnucmat.2018.08.010.
[17] Nishi, T., Manako, T., Ohnuma, K., Ohta, H., Sukenaga, S., Shibata, H., and Oniki, T. *J. Nucl. Sci. Technol.*, **0** (2019), 1, https://doi.org/10.1080/00223131.2019.1617206.
[18] Shurygin, P. M., Buzovkin, V. P., and Leonov, V. V., *Teplofiz. Vysok. Temp.*, **14** (1976), 1101.
[19] Kim, Y., and Morita, K. *J. Am. Ceram. Soc.*, **98** (2015), 1588, https://doi.org/10.1111/jace.13490.

[20] Nilsson, O., Sandberg, O., and Bäckström, G. *Int. J. Thermophys.*, **6** (1985), 267, http://dx.doi.org/10.1007/BF00522148.
[21] Botta, W. J., Ota, K., Hajlaoui, K., Vaughan, G., and Yavari, A. R. *J. Non-Cryst. Solids*, **354** (2008), 325, https://doi.org/10.1016/j.jnoncrysol.2007.07.043.
[22] Southard, J. C. *J. Am. Chem. Soc.*, **63** (1941), 3147, https://doi.org/10.1021/ja01856a073.
[23] Gutzow, I. S., Mazurin, O. V., Schmelzer, J. W., Todorova, S. V., Petroff, B. B., and Priven, A. I., *Glasses and the Glass Transition*, John Wiley & Sons, 2011, https://doi.org/10.1002/9783527636532.
[24] Ogura, G., Suh, I.-K., Ohta, H., and Waseda, Y. *J. Ceram. Soc. Jpn.*, **98** (1990), 305, https://doi.org/10.2109/jcersj.98.305.
[25] Carslaw H. S, Jaeger, J. C. *Conduction of Heat in Solids.* Oxf. Clarendon Press; 1959.
[26] Napolitano, A., Macedo, P. B., and Hawkins, E. G. *J. Am. Ceram. Soc.*, **48** (1965), 613, https://doi.org/10.1111/j.1151-2916.1965.tb14690.x.
[27] Baehr H. D, Stephan K. *Wärme-Und Stoffübertragung*, Springer; 1996, https://doi.org/10.1007/978-3-642-10194-6.
[28] *National Astronomical Observatory of Japan: Chronological Scientific Tables*, Maruzen; 2017.
[29] https://www.plansee.com/ viewed 2019-03-18.
[30] Edwards, J. W., Speiser, R., and Johnston, H. L. *J. Appl. Phys.*, **22** (1951), 424, https://doi.org/10.1063/1.1699977.
[31] Dubberstein, T., Heller, H.-P., and Scheller, R. P. *Proceedings of the Ninth International Conference On Molten Slags, Fluxes and Salts*, (2012), https://doi.org/10.1179/03019233 12Z.000000000163.
[32] Glaser, B., and Sichen, D., *Metall. Mater. Trans. B*, **44** (2013), 1, https://doi.org/10.1007/s11663-012-9773-9.
[33] Ozawa, S., and Susa, M. *Ironmak. Steelmak.*, **32** (2005), 487, https://doi.org/10.1179/174328105X48179.
[34] Yamasue, E., Susa, M., Fukuyama, H., and Nagata, K. *Metall. Mater. Trans. A*, **30** (1999), 1971, http://dx.doi.org/10.1007/s11661-999-0007-y.
[35] Riebling, E. F. *J. Am. Ceram. Soc.*, **49** (1966), 19, https://doi.org/10.1111/j.1151-2916.1966.tb13139.x.
[36] Mackenzie, J. D. *J. Phys. Chem.*, **63** (1959), 1875, https://doi.org/10.1021/j150581a021.
[37] Thomas, S. B., and Parks, G. S. *J. Phys. Chem.*, **35** (1931), 2091, https://doi.org/10.1021/j150325a016.
[38] Kittel, C. *Phys. Rev.*, **75** (1949), 972, https://doi.org/10.1103/PhysRev.75.972.
[39] Grimsditch, M., Bhadra, R., and Torell, L. M. *Phys. Rev. Lett.*, **62** (1989), 2616, https://doi.org/10.1103/PhysRevLett.62.2616.
[40] Macedo, P. B., Capps, W., and Litovitz, T. A. *J. Chem. Phys.*, **44** (1966), 3357, https://doi.org/10.1063/1.1727238.
[41] Kodama, M. J. *Non-Cryst. Solids*, **127** (1991), 65, http://dx.doi.org/10.1016/0022-3093(91)90401-Q.